Title
A lateral electrophoretic flow diagnostic assay

Journal
Lab on a Chip, 15(6)

ISSN
1473-0197

Authors
Lin, Robert
Skandarajah, Arunan
Gerver, Rachel E
et al.

Publication Date
2015-03-21

DOI
10.1039/c4lc01370k

Peer reviewed

Lab on a Chip

PAPER

View Article Online
View Journal | View Issue

Cite this: *Lab Chip*, 2015, **15**, 1488

A lateral electrophoretic flow diagnostic assay†

Robert Lin,‡[a] Arunan Skandarajah,[b] Rachel E. Gerver,[b] Hector D. Neira,[b] Daniel A. Fletcher[ab] and Amy E. Herr*[ab]

Received 20th November 2014,
Accepted 13th January 2015

DOI: 10.1039/c4lc01370k

www.rsc.org/loc

Immunochromatographic assays are a cornerstone tool in disease screening. To complement existing lateral flow assays (based on wicking flow) we introduce a lateral flow format that employs directed electrophoretic transport. The format is termed a "lateral e-flow assay" and is designed to support multiplexed detection using immobilized reaction volumes of capture antigen. To fabricate the lateral e-flow device, we employ mask-based UV photopatterning to selectively immobilize unmodified capture antigen along the microchannel in a barcode-like pattern. The channel-filling polyacrylamide hydrogel incorporates a photoactive moiety (benzophenone) to immobilize capture antigen to the hydrogel without *a priori* antigen modification. We report a heterogeneous sandwich assay using low-power electrophoresis to drive biospecimen through the capture antigen barcode. Fluorescence barcode readout is collected *via* a low-resource appropriate imaging system (CellScope). We characterize lateral e-flow assay performance and demonstrate a serum assay for antibodies to the hepatitis C virus (HCV). In a pilot study, the lateral e-flow assay positively identifies HCV+ human sera in 60 min. The lateral e-flow assay provides a flexible format for conducting multiplexed immunoassays relevant to confirmatory diagnosis in near-patient settings.

Introduction

Immunoassays have played a critical role in diagnostics for more than five decades.[1] Enzyme-linked immunosorbent assays (ELISAs) and lateral flow assays are often the "go-to" tool for screening diagnostic questions.[2,3] A prevalent diagnostic paradigm is use of a disposable assay in conjunction with a costly, though reusable, reader device.[4–6] Widely available mobile communication devices have emerged as feasible detectors for some screening scenarios (*e.g.*, cell and smart phones).[7–10] With quality optics and sophisticated sensors in phones, mobile devices can acquire high quality images and transmit results to or from remote sites. Further, use of commercially available re-appropriated mobile devices as readers mitigates maintenance, upkeep, and repair of stand-alone specialty instruments in low-resource settings.

In tandem with healthcare advances employing mobile communication devices, microanalytical systems are gaining relevance to near-patient diagnostic questions.[11–13] A variety of immunoassays have been developed that benefit from small sample volume requirements, reduced reaction times and precise flow and reaction control.[14–17] Microfluidic assays have been demonstrated with mobile imaging readouts.[18–21] The assay and reader technologies are complementary. First, the compact form factor of both microfluidic devices and smartphone-based imaging is well-suited to point-of-care use. Second, optically transparent microfluidic devices are widely used (*e.g.*, elastomers, glass and plastics) and compatible with optical detection by phone-based diagnostic systems. Third, the use of a reader instrument increases the utility of low-volume microfluidic assay, including heterogeneous immunoassay formats, as visual readout can be a challenge in near-patient settings. Lastly, and importantly to high clinical sensitivity and specificity performance, imaging of a complete field of view (in contrast to single point detection) is suited to multiplexed heterogeneous assays (*e.g.*, HCV assays). To this end, we adopt a barcode-format – patterned reactive bands – analogous to commercially available confirmatory diagnostic tests (*i.e.*, immunoblot strip).

Photopatterning of capture antigens is a prime way developers create multiplexed immunoassays in microfluidic devices.[22] Proteins can be immobilized on microchannel surfaces *via* covalent interactions.[23–27] Nevertheless, immobilization on bare channel surfaces does require grafting of reactive groups onto the surface and/or the use of linkers to attach proteins to the surface. A low percentage of proteins from the bulk solution (as low as 0.01%) are typically

[a] *Department of Bioengineering, UC Berkeley, Berkeley, CA 94720 USA. E-mail: aeh@berkeley.edu*
[b] *UC Berkeley/UCSF Graduate Program in Bioengineering, UC Berkeley, Berkeley, CA USA, and University of California, San Francisco, San Francisco, CA USA*
† Electronic supplementary information (ESI) available: Data regarding validation of barcode patterning and photo-bleaching studies. See DOI: 10.1039/c4lc01370k
‡ Robert Lin is now at Cepheid.

immobilized onto the reactive (2D) surface.[28] The low surface immobilization efficiency is partially attributable to confinement of reactions to surfaces and to competing and, sometimes, interfering transport phenomena (*e.g.*, mass transport limits). The use of polymer monoliths and reactive (3D) volumes can surmount limitations by yielding a pseudo-homogeneous reaction system (in contrast to purely heterogeneous systems that may suffer from depletion regions).[29–34] Further, monoliths provide increased surface area for the immobilization of proteins, as compared to reactive channel wall surfaces. Hydrogels have also been used to immobilize reactive species, with some systems relying on the dense gel matrix to physically trap the proteins.[35–38] In a variation, biotinylated capture antigens were immobilized on streptavidin-functionalized hydrogel structures.[39] Unfortunately, the technique involves a blocking step that leads to long processing times when creating complex patterns.

We demonstrate a barcode sandwich immunoassay conducted in a single, hydrogel-filled microchannel housed in a glass microfluidic device. To expedite fabrication and afford the possibility of multiplexing (barcode layout) in this simple geometry, we employ a recently described photopatternable polyacrylamide gel – termed a light-activated volume-accessible gel (LAVAgel)[40] – as the 3D immobilization matrix. Low power electrophoresis drives target antigens to the immobilized capture sites in the hydrogel. The assay consumes only milliwatts of power during operation, potentially compatible with miniaturized instrumentation. For brevity, we adopt the shorthand nomenclature "lateral e-flow" to describe the format.

In this proof-of-concept lateral e-flow assay, we focus on confirmatory (not screening) diagnosis of hepatitis C viral (HCV) infection. For context, HCV affects 150 million people worldwide and causes more than 10 000 deaths in the US alone. To aid in HCV confirmatory diagnosis efforts, a lateral e-flow assay for sera levels of antibodies against the HCV antigens c33c, c100p and c22p is reported as a proof-of-principle. The HCV lateral e-flow assay is used in conjunction with a fluorescence-enabled mobile imaging system – the CellScope[10,41] (Fig. 1a). A different implementation of the CellScope platform is currently under field-testing for fluorescence-based detection of tuberculosis in sputum smears.[42] Taken together, the barcode lateral e-flow assay comprises an alternate confirmatory diagnostic tool.

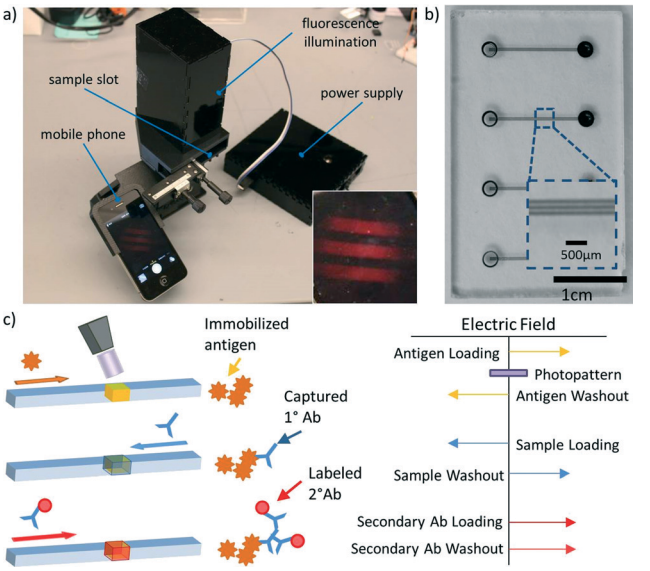

Fig. 1 Lateral e-flow assay concept. a) Photograph of the fluorescence-enabled CellScope with an iPhone 4S as the imaging modality. (Phone shows actual image of chip inside the CellScope) Inset: enlarged view of phone screen, showing fluorescence image. b) Photograph of microfluidic chip with 4 (devices) well-pairs each connected by 3 microfluidic channels. Inset: zoomed-in image of 3 parallel microfluidic channels. c) Conceptual schematic of e-flow assay implementation. Antigen is immobilized on the LAVAgel using photopatterning and sample is introduced to capture primary antibodies. Labeled secondary antibodies are used to identify captured primary antibodies and provide signal amplification.

Materials and methods

Chemicals and reagents

Aqueous solution of 30% (w/v) (29 : 1) acrylamide/bis-acrylamide, glacial acetic acid, ammonium persulfate (APS), *N*,*N*,*N*′,*N*′-tetramethylethylenediamine (TEMED), methanol and 3-(trimethoxysilyl)-propyl methacrylate and sodium hydroxide (NaOH) were purchased from Sigma-Aldrich (St. Louis, MO). *N*-[3-[(4-Benzoylphenyl) formamido-[propyl]-methacrylamide (BPMAC) was custom synthesized by PharmAgra Labs (Brevard, NC). AlexaFluor 488 (AF488) and AlexaFluor 555 (AF555) labeled Ovalbumin (OVA) and bovine serum albumin (BSA) were purchased from Life Technologies (Carlsbad, CA). FITC-labeled anti-BSA antibody was purchased from MyBiosource Inc. (San Diego, CA). Hepatitis-C Virus (HCV) positive serum, AF488 conjugated HCV Core (c22p), NS3 (c33c) and NS4 (c100p) antigens were kindly provided by Novartis Diagnostics (Emeryville, CA). HCV negative human sera were purchased from SeraCare Life Sciences (Oceanside, CA). HCV-positive human sera were provided as a gift by Novartis Diagnostics (Emeryville, CA). AlexaFluor 568 (AF568) conjugated secondary goat anti-human antibody was purchased from Life Technologies (Carlsbad, CA). All antigen, antibody and serum samples were diluted into 1× Tris-glycine buffer before introduction into the chip. 1× Tris-glycine buffer was purchased at 10× concentration from Bio-Rad (Hercules, CA).

Data acquisition, control and patterning instrumentation

During assay development, images were acquired on an Olympus IX-50 inverted fluorescence microscope (Olympus USA, Center Valley, PA) using a Peltier-cooled CCD camera CoolSNAP HQ2 (Roper Scientific, Trenton, NJ) through a 10×/0.3 NA objective (Olympus USA, Center Valley, PA). A green fluorescence channel Omega XF100-3 filter cube and red fluorescence channel XF102-2 filter cube (Omega Optical, Brattleboro, VT) were used. Exposure times were 150 ms and

300 ms respectively (unless otherwise specified). Illumination was provided by an X-cite exacte illumination system from Lumen Dynamics (Mississauga, Canada) controlled using Metamorph software from Molecular Devices (Sunnyvale, CA). Image analysis and stitching of multiple adjacent microscope images was performed using ImageJ from NIH (Bethesda, MD). A custom-built programmable high-voltage power supply (HVPS) was used for electrophoretic control with platinum electrodes directly inserted into the sample reservoir wells. UV for photopatterning was provided by a Hamamatsu Lightningcure LC5 unit (Bridgewater, NJ) through a Lumatec series 380 liquid light guide (Deisenhofen, Germany). Photomask designs were created in-house and laser cut from 50 μm thick stainless steel sheet using Universal Laser PLS6MW with a 30 W fiber laser cartridge (Scottsdale, AZ).

Microfluidic chip preparation

Chips were designed in-house and glass chip fabrication was performed by Perkin Elmer (Hopkinton, MA). Standard wet etching and drilling methods were used followed by thermal bonding.[43] Each device consists of three parallel microfluidic channel of 1.2 cm length, 90 μm width and 20 μm depth connecting wells of 2 mm in diameter and 1 mm deep that serves as the sample reservoirs. Each chip contains 4 devices with 3 channels each (Fig. 1b).

Prior to introduction of polyacrylamide gel precursor solutions the glass channel surfaces were functionalized with an acrylate-terminated self-assembled monolayer.[44] Precursor solution with 1× TG, 4% wt/vol total acrylamide (4% T) with 2.6% of the total as cross-linker bisacrylamide (2.6% C) and 1.6 mM BPMAC were mixed and degassed with sonication and vacuum. The BPMAC imparts photo-activatable capture capability to the polyacrylamide gel. Immediately prior to introduction into the device 0.08% (wt/vol) of APS and 0.08%(vol/vol) of TEMED were added to the precursor solution to initiate polymerization. Wells were flushed twice with 1× TG buffer after 15 min of polymerization then filled with 1× TG buffer and stored in a humidified petri dish at 4 °C. Gelation was confirmed by examining excess precursor solutions prior to well rinsing.

Barcode assay fabrication

Protein bands were photopatterned (barcodes) inside the microfluidic channels after completion of chip and gel preparation. Briefly, proteins (labeled or unlabeled) were diluted into 1× TG buffer and the solution was pipetted into the sample wells (~6 μL). Sample was then electrophoretically loaded into the microfluidic channel by applying a 200 V electrical bias between the sample and waste wells. Barcode proteins were loaded for two minutes, an empirically derived time allowing proteins to be uniformly loaded into the channels. After loading, the photomask was aligned with the channel structures, and the light guide was placed directly on top of the opening and in contact with the mask. Subsequently, UV illumination was applied for 5 s at 20% diaphragm opening controlled through the instrument interface. After illumination the wells were each rinsed three times with 1× TG buffer and a reverse bias of 500 V was applied for 5 min to electrophoretically wash out non-immobilized proteins. Protein band patterning was confirmed through fluorescence imaging.

HCV lateral e-flow assay workflow

Sample reservoirs are rinsed with 1× TG buffer 3× before serum samples are pipetted onto the chip and electrophoresed into the microfluidic channels initiating the assay. Dilute sera (1 : 40) were loaded for 15 min at a 200 V bias followed by an electrophoretic washout step at 200 V reverse bias for 20 min. The sera were diluted to facilitate the electrophoretic loading of the sample. As is typical in immunoassays, sample dilution is necessary to reduce or eliminate sample matrix interference effects. In the lateral e-flow assay, matrix effects extend beyond potential interference with the detection regents to also include interference with the support hydrogel itself (*i.e.*, gel pore clogging), as described previously.[45] Immunoprobing of captured human anti-HCV antibodies is performed by introducing fluorescently labeled anti-human antibodies for 10 min at 200 V bias followed by washout at 200 V for an additional 10 min. Fluorescence micrographs capture the blotting result. To assess assay readout signal, area under the curve (AUC) values were computed for each barcode element from the fluorescence micrographs and CellScope micrographs (ImageJ). An SNR of >3 was used as the detection criterion in the HCV detection assays.

Mobile microscope design

The CellScope fluorescence microscope consists of a transmission light path capable of fluorescence and bright-field illumination and a finite conjugates imaging pathway built into a 3D printed casing designed to couple to an iPhone 4S, a modification to previously reported devices.[10,41] The collection optics include a 10×/0.25 NA objective (Edmund Optics, Barrington, NJ, #36-132) spaced 160 mm from a 20× wide field eyepiece (#39-696) with a pair of silver turning mirrors (CM1-P01, Thorlabs, Newton, NJ,) yielding a compact form factor. The casing, stage, and phone adapters were printed using thermally extruded ABS plastic utilizing a desktop 3D printer (uPrint Plus, Stratasys, Eden Prairie, MN,). Illumination for the simultaneous dual-colour fluorescence employs a mounted Rebel Neutral White (4100 K) LED purchased from LuxeonStar (MR-WN090-20S, Brantford, ON, CA) attached to a heat sink (294-1111-ND, Digikey, Thief River Falls, NY,). An aspheric lens (KPA031, Newport, Irvine, CA) with a diameter of 25 mm and 17 mm effective focal length is offset from the LED by one focal length and used as a collector lens with a second asphere of the same type used as a condenser lens.

The dual band-pass excitation filter (59022x, Chroma Technology, Bellows Falls, VT) after the collector selects two excitation bands centered at 470 nm and 570 nm from the collimated source. After the excitation filter, a

coverslip set at 45° couples in light from a standard 5 mm green LED for bright-field imaging of the chip. The condenser lens then focuses the light on the sample plane. An emission filter (59022m, Chroma Technology, Bellows Falls, VT) is placed as close as practical to the back focal plane of the objective to select emission bands centered at 520 nm and 630 nm. A separate modular enclosure contains a rechargeable lithium ion battery (Astro Pro External Battery, Anker), a 700 mA BuckPuck DC Driver (3023-D-E-700, Luxeon Star, Brantford, ON, CA), and a switch for selecting between fluorescence and bright-field illumination. Final spectral separation of spatially overlaid fluorescent probes uses the on-board Bayer filter on the phone which, in combination with an on-board demosaicing algorithm, assigns a red, green, and blue value to each pixel. Imaging uses the default camera application on the iPhone 4S with the exposure time and focus locked on a dark field to maximize sensitivity.

Results and discussion

Antigen 'barcodes' for the lateral e-flow architecture

We developed a rapid protocol for immobilizing spatially varying concentrations of reagents inside of a simple, straight microfluidic channel. Use of photomasking enables exposure of select microchannel regions to UV light and, thus, limits activation of the LAVAgel to those exposed regions through the BPMAC monomer. Once immobilized, the capture antigen forms the basis for a sandwich immunoassay addressed by electrophoresis (Fig. 1c).

The light patterning methodology requires neither modification of the capture antigen (*i.e.*, no biotinylation) nor blocking steps during barcode fabrication, thus simplifying the fabrication process. Each patterning cycle is divided into three steps and can be repeated to create complex patterns. To create the barcode, capture antigen is electrophoresed into the LAVAgel. Once the channel is filled with antigen, a photomask is placed on top of the chip and UV illumination is applied. The photomask has open slits which allow UV transmission, resulting in narrow slit-like regions of LAVAgel activation. In regions exposed to UV light, capture antigen is covalently linked to the LAVAgel.[46] Subsequent electrophoretic washout leaves bands of captured labeled protein on the hydrogel, while proteins from masked regions proteins migrate freely out of the gel. (Fig. 2a) The process of load-pattern-wash is repeated (with different proteins and masks) to pattern a barcode in concentration of capture antigens along the axis of the microfluidic channel. For example, repeating the patterning cycle three times results in a barcode pattern with five capture antigen bands comprised of three unique proteins. The total time to fabricate a 5-plex immobilized antigen barcode (with non-reactive separation spacer regions interleaved) was 35 minutes with 3 steps per barcode region. This compares favorably to other single-channel barcode approaches that rely on functionalized capture antigens

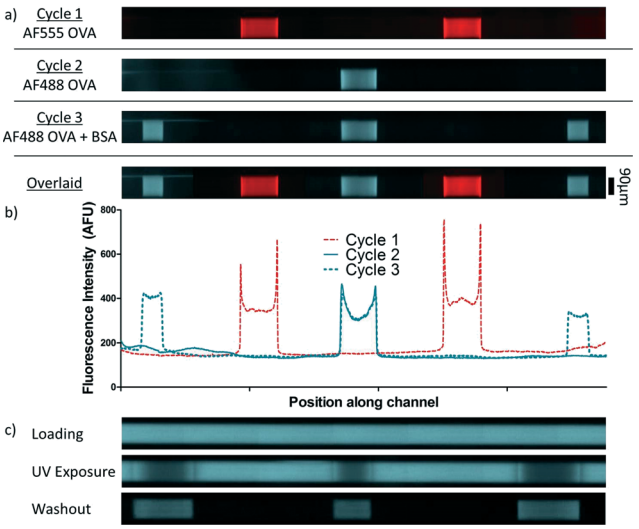

Fig. 2 Fabrication of multiplexed antigen barcode for lateral e-flow assay device. a) Cycle 1: two bands of OVA-AF555 were concurrently photo-patterned. Cycle 2: a single band of OVA-AF488 was photo-patterned. Cycle 3: two BSA-AF488 bands were photo-patterned. Overlaid composite image reports all 5 immobilized bands. b) Fluorescence signal traces show reduced levels at the center of immobilized bands, attributed to photo-bleaching. c) Fluorescence micrograph reveals significant photo-bleaching after UV exposure.

and streptavidin-containing polymers (60 minutes with 51 total steps).[39]

We first sought to identify and characterize nonspecific interaction of capture proteins with the LAVAgel matrix during fabrication of a multiplexed barcode (Fig. 2). As a test system, we first photopatterned AF555-labeled OVA, then AF488-OVA, and finally AF488-BSA. (Fig. 2a) Inspection of the spacer regions between capture antigen bands showed no change in fluorescence signal throughout the patterning process, suggesting limited non-specific immobilization in unexposed areas of the gel (Fig. 2b).

We observed no measurable change in fluorescence signal in the AF488 spectral channel at the central band (AF488-OVA) between cycles 2 and cycle 3, as demonstrated by the complete overlap in the profile plot. This observation suggests minimal nonspecific interaction of capture antigens with previously activated LAVAgel.

Spatial resolution of the photopatterning method was also assessed with minimum band widths of ~200 μm and minimum spacing between proteins bands at ~250 μm. The widths of the patterned proteins bands are observed to be ~4.5× that of the width of mask slit width. One potential cause for the larger size of the exposed region could be the use of a non-collimated UV illumination source that results in UV-activated regions that are wider than defined by the mask. Note that even a collimated light source would have a finite divergence angle yielding a patterned band wider than the mask slit width.

We next characterized the immobilization efficiency by fabricating barcodes of AF488-labeled BSA (Fig. 2c). We measured fluorescence signal from capture antigen (labelled with

a fluorophore) throughout the patterning process. In comparing UV exposed regions before and after UV exposure, we observed a 51.1% (±1.1%; n = 6) decrease in fluorescence signal. The signal decrease is attributed to UV photo-bleaching of the AF488 dye and not to loss of protein mass since there has been no wash step between these measurements. In accordance with use of an un-collimated UV source, we further observed non-uniform photo-bleaching across the 550 μm long band of labelled antigen. The non-uniform photo-bleaching at the edge of the bands (Fig. 2c) likely arises from diffraction.

After electrophoretic washout of mobile proteins, fluorescence signal measured at UV exposed locations shows immobilization of 84.6% (±1.4%; n = 6) of the available protein. Immobilization efficiencies were calculated by comparing fluorescence levels at the center of each band. Specifically, a 20 μm region was selected from the center of each of the 6 photopatterned bands. The mean fluorescence signal from the region was calculated for both the post-UV exposure signal and the post-washout signals. The mean fluorescence value from post-washout was then divided by the fluorescence value after UV exposure to calculate the immobilization efficiency for each of the 6 locations. Given detectable UV photo-bleaching, comparison of signal from the post-UV exposure conditions to signal after electrophoretic washout was used. The ~85% photo-capture efficiency compares favorably against the ~0.01% efficiency observed in surface-based immobilization[28] and is in line with the 75–97% capture efficiency reported with previous photo-activatable polyacrylamide gel-based protein capture.[47]

As we observed non-uniform photo-bleaching of the fluorescence signal, we characterized the distribution of immobilized protein across the band using antibody probing. We patterned unlabeled BSA along with fluorescently labeled OVA and probed for BSA using fluorescently labeled antibodies. (Fig. S1, ESI†) The patterned OVA band shows clearly the photo-bleached center whereas the primary and secondary probe results of the patterned BSA band reveals a distribution that is high in the center and low on the edge. This is in line with our expectation as we observed elevated UV dose at the center based on observed non-uniform photo-bleaching. Although higher UV dose resulted in high photo-capture, excess UV dosage results in band patterns that are no longer well defined. High UV illumination (both in power and time) results in broadened bands due to activation of neighboring benzophenone groups by excess radicals.[46]

Detection of antibody *via* photo-immobilized capture proteins

We next evaluated the performance of antigen–antibody binding with capture antigen covalently immobilized (*via* benzophenone) to the hydrogel matrix. An OVA and anti-OVA pair was assessed. Anti-OVA was labelled with AF568 for monitoring. 5.5 μM of unlabelled OVA plus 50 nM OVA-AF488 and 5.5 μM BSA plus 50 nM BSA-AF488 (negative control) were photocaptured to the gel. After immobilization of the OVA and BSA bands, a dilute solution of AF568-labeled anti-OVA antibody (~70 pM) was electrophoresed into the channel (Fig. 3a), from the right hand side of the micrographs. Over the 125 min load time, signal accumulates at the location of the immobilized OVA, with bias towards the right side of that band (Fig. 3b), indicating a transport limited system. Minimal antibody signal is detectable after 120 min of loading at the location of an immobilized off-target protein (BSA).

Signal accumulated at the patterned region was measured as the sum of pixel intensities over the patterned band location for both the on-target and off-target locations. As shown in Fig. 3c, at the location of the immobilized OVA, the signal continually increases during the loading period whereas at the off-target protein location the signal is only detectable after 30 minutes of loading and then reaches a low plateau that remains constant after 90 minutes. Antibody–antigen binding reaction is understood to behave according to first-order binding kinetics, governed by the dissociation constant of the reaction – K_d. First-order binding kinetics are expected when one component is in excess, as is the case for the immobilized antigen in the lateral e-flow assay. Product – in this case the bound antibody–antigen complex at the band location – accumulates exponentially. We applied an exponential fit to the time-dependent SNR and observed good agreement between the fit and the data (R^2 = 0.9901). As the assay operates in a transport limited regime when the immobilized capture antigen is patterned at a high concentration relative to the sample, the k_{on}/k_{off} values cannot be directly calculated from these experimental data. The first-order

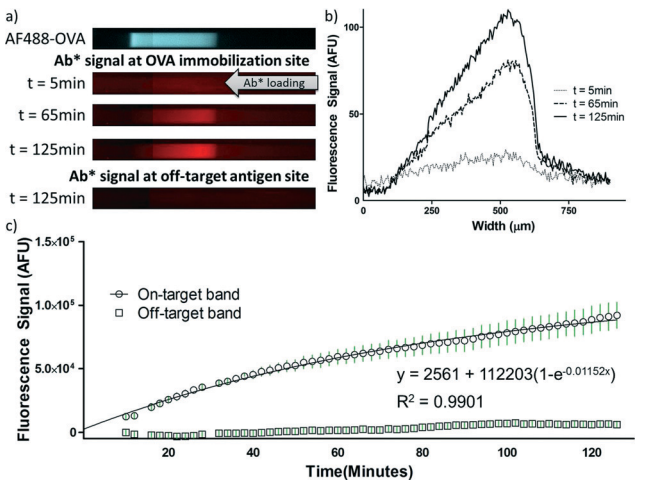

Fig. 3 Direct immunoassay for target antibody detection *via* covalently immobilized protein partner. a) Micrograph of immobilized OVA-AF488 and time course of on-target signal during loading of dilute (~70 pM) antibody sample. Off-target BSA band at t = 125 min. b) Line plots of signals at the patterned OVA band at times = 5, 65 minutes and 125 minutes, E = 300 V cm^{-1}. c) Captured antibody fluorescence signal at capture OVA location (open circle) with exponential fit (solid line). Signal plotted is the average of 3 parallel channels with vertical green line showing 1 standard deviation of the measured signal. Signal is the sum of pixel values over a 180 μm region of interest (ROI) minus the sum of pixel values over a channel region of same ROI with no immobilized proteins.

curve fit depends on the electrophoretic velocity of the antibody through the gel, as well as on the k_{on}/k_{off} values of the antibody–antigen pair.

The signal-to-noise ratio (SNR) was calculated using:

$$\mathrm{SNR} = \frac{\mathrm{Signal}}{\sqrt{(\mathrm{Shot\ Noise})^2 + (\mathrm{Random\ Noise})^2 + (\mathrm{Dark\ Noise})^2}}$$

adapted from Dussault and Hoess.[48] The signal is calculated as the background-subtracted signal and the shot noise is the square-root of the signal. For this calculation the random noise and dark noise is lumped together as the standard deviation of pixel intensities measured at a region where no proteins were patterned – the inherent variation in the measurements. The increase in the SNR is similar to the increase in the measured total signal, reaching a maximum SNR of ~140 at the end of the 2 hour loading period (Fig. 4a). As SNR is still increasing at 2 hours, the results suggest that longer loading times and/or higher electric fields, to increase transport, would lead to even higher SNR, enabling lower limits of detection for the assay. At 5 min after initial loading, the SNR at the on-target band is ~21, suggesting that rapid diagnostic tests are feasible. Further optimization would vary the electrophoretic velocity to control the Damköhler number as suggested by Araz *et al.*[39] For instance, by fine-tuning the electrophoretic transfer rate to ensure the assay operates in the transport-limited regime while minimizing assay times.

The majority of signal accumulates at one side of the patterned protein band (Fig. 3b). With a low sample concentration in a transport limited regime, a depletion zone behind the initial binding region is created as the analyte becomes consumed.[49] In this regime, the majority of target antibody in the sample can be captured and quantified.[48]This suggests that for low concentration targets a wide band is not necessary to maximize SNR. This optimization reduces protein consumption, an often costly component in point-of-care diagnostic tests. Although a larger patterned band would capture more total analyte, an increase in SNR would not necessarily follow, as the total random and dark noise will scale linearly with increasing region of interest (ROI). We characterize this behavior by examining the maximum SNR as a function of the size of the ROI over which the signal is calculated (Fig. 4b). As ROI size increases, the signal will increase and the ratio of signal to shot noise will increase as the square root of the signal. On the other hand, the random and dark noise will increase linearly with increasing ROI size. These competing factors lead to a band width that maximizes overall SNR in the system. The SNR for the current study reaches a maximum at an ROI width of 180 μm. Previous characterization of antibody–antigen binding using the photo-capture approach employed in the barcode assay showed K_d in agreement with literature K_d values determined by SPR for the same protein and antibody pair (PSA and anti-PSA).[50] The k_{off} for the binding pair was roughly an order of magnitude lower by SPR, with the major caveat that the buffer pH was different between the two systems studied.

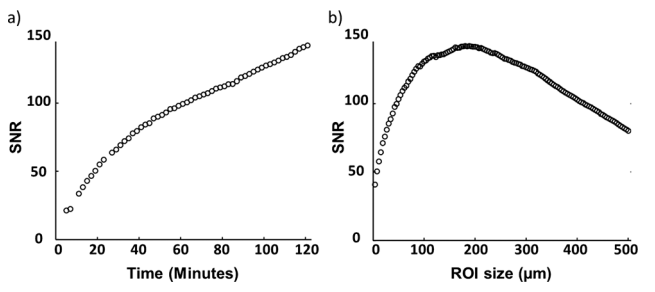

Fig. 4 Signal-to-noise ratio (SNR) increases over time and can be used to guide device design. a) SNR increases over the time course of sample loading. b) Barcode design can be optimized based on immobilized protein band size that leads to maximum SNR. Peak SNR is observed by measuring the first 180 μm of band width.

Lateral e-flow for HCV in human sera

We developed and characterized a lateral e-flow barcode immunoassay for hepatitis C virus (HCV) in diluted human sera (Fig. 5a). The barcode consisted of a five band pattern including three AF488-labeled HCV antigens, one negative control (UV only) and one positive control (protein L). The three HCV antigens included c100p (a peptide fragment from

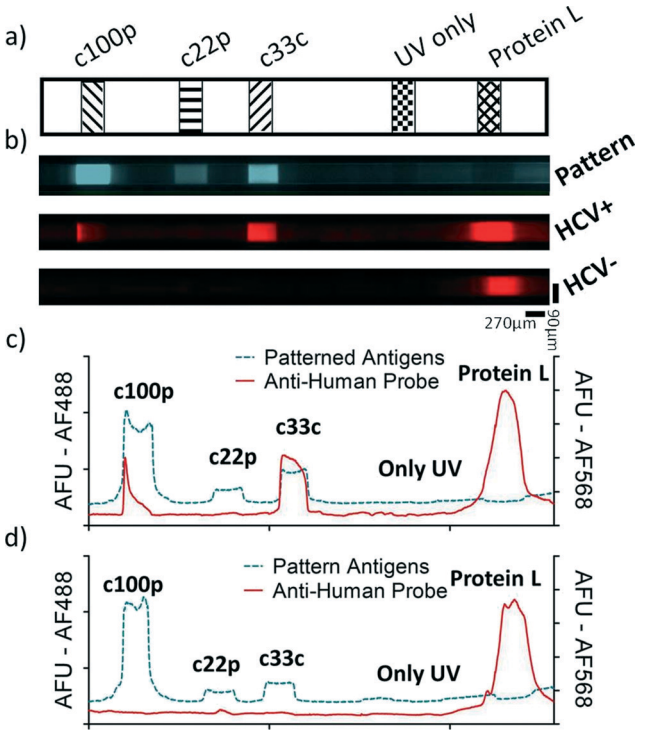

Fig. 5 Human serum HCV lateral e-flow assay. a) HCV barcode assay comprised of 3 HCV antigen bands (c100p, c22p, c33c), negative control (UV only) and positive control (protein L) bands. b) Fluorescence micrographs show HCV barcode pattern (HCV antigens labelled with AlexaFluor 488, UV only and protein L are not labelled). Lateral e-flow assay readouts for HCV+ and HCV– human sera. Corresponding fluorescence traces for HCV+ (c) and HCV– (d) sera results.

NS4 – a membrane binding protein), c22p (a peptide from core protein) and c33c (a viral protein NS3 – a recombinant virus protease). The three HCV antigens are members of an antigen panel used in commercial recombinant immunoblot assay (RIBA) HCV confirmatory diagnostic assays and are used to confirm the serum presence of antibodies against the virus. As a positive (loading) control, protein L is a bacterial protein that binds to human immunoglobulins. For assay development, the three HCV antigens were labeled with a fluorophore. Neither protein L (unlabeled) nor the UV exposed site emitted fluorescence, as expected.

In a pilot study, diluted sera classified as highly reactive (HCV+) and non-reactive (HCV−) using a commercially available RIBA assay were assessed with the lateral e-flow device. The confirmatory RIBA immunoblot strip is based on the western blotting assay, with HCV recombinant antigen bands immobilized on membranes. To complete the RIBA, the membranes are incubated with patient sample (serum or plasma) and human antibodies against each antigen detected using peroxidase-labeled anti-human IgG and colorimetric detection (*e.g.*, 4-chloro-1-naphthol).[51] RIBA sample scoring utilizes primarily reactive band intensity, relative to control band, when reactive bands number at two or more. Indeterminate results remain problematic, even with refinement of recombinant antigen band composition.[51] RIBA scored the HCV+ serum assayed here as 4+ on the c100p, c33c and c22p bands at 1 : 50 dilution. Sera were diluted off-chip 1 : 40 (1× Tris-glycine buffer) and then electrophoretically loaded into the HCV diagnostic device for 15 min followed by 20 min of electrophoretic washout with the 1× Tris-glycine buffer. The volume of human serum consumed per triplicate assay was ~150 nL. Note that a typical human finger prick procedure yields ~20 μL of blood. The total assay duration was 60 minutes, which compares favorably with the minimum 4 h gold-standard RIBA for HCV currently in use.[52,53]

For detection, a secondary antibody (71.5 nM; goat anti-human) was then electrophoretically introduced into the lateral e-flow channel (10 min load; 10 min washout). The lateral e-flow HCV barcode was imaged using an inverted epi-fluorescence microscope. The HCV+ serum yielded secondary antibody signal at both the c100p and c33c antigen locations in addition to the protein L band, suggesting the serum contains human antibodies that react with the patterned viral proteins – indicative of HCV infection (Fig. 5c). The secondary signal aligns well with the location of the immobilized c100p and c33c antigens, suggesting specific interactions of human antibodies. The region with only UV illumination shows no signal indicating no nonspecific interaction with the activated gel. We observed no secondary antibody signal at the c22p location and attribute the observation to the low quantity of antigen immobilized, as suggested by the low fluorescence level measured at antigen patterning. The human HCV− serum yielded signal from the secondary detection antibody only at the protein L location, thus suggesting successful sample loading but no reactivity of the sample with HCV antigen (Fig. 5d). Empirically determined power requirements for the lateral e-flow system suggest the system can operate using three 9 V batteries driving both the electrophoresis steps and the imaging step.

Lateral e-flow HCV assay and CellScope imaging

Finally, we imaged the HCV lateral e-flow device with a customized fluorescence-capable CellScope (Fig. 1a). The CellScope instrument adapts camera phones to function as the image acquisition component of a simple transmission microscope. Thus, the tool provides high resolution imaging in a portable format, while taking advantage of illumination uniformity through an LED source and recent improvements in mobile phone camera sensitivity. In the customized CellScope employed here, a white light LED illumination source was paired with both a dual band-pass filter set and the built-in Bayer filter array of a mobile phone (iPhone 4S) to collect multi-color fluorescence signal. A schematic depicting the light path inside the fluorescence CellScope is shown in Fig. 6a. Per this approach, each barcode band was

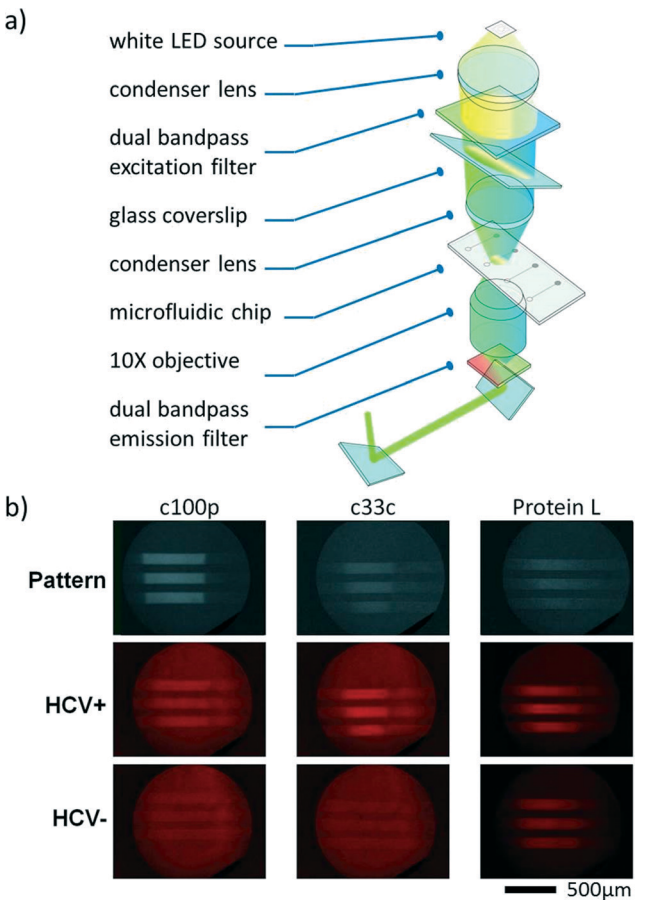

Fig. 6 Mobile imaging device for diagnostic data acquisition. a) Schematic showing the light path inside the customized fluorescence CellScope. b) Lateral e-flow readouts using fluorescence-enabled CellScope. The RGB image acquired from the smartphone was split into 3 separate spectral channels. Lateral e-flow assays and samples correspond to Fig. 5a.

imaged simultaneously in the green and red spectral channels, underpinning ready spatial correlation of the capture antigen and detected antibody fluorescence signals. No switching of spectral filters or illumination sources was needed.

CellScope imaged the c100p, c33c and protein L bands of the HCV lateral e-flow assay for the patterned antigens, and secondary antibody probe signal of both HCV+ and HCV− sera (Fig. 6b). The system was designed to capture a circular field of view inscribed on the rectangular sensor of the mobile phone.

Imaging required approximately 3 minutes per lateral e-flow assay. Comparison between the HCV lateral e-flow assay imaged with epi-fluorescence microscopy to imaging with the portable CellScope modality shows promising qualitative performance. Both systems offered the analytical sensitivity to detect c100p and c33c, in highly reactive human sera and protein L in both HCV−/HCV+ sera. Further, the CellScope provided the spatial resolution needed to detect the separate capture antigen bands in the microchannels. This pilot study shows promise for implementing a purely electronic, lateral e-flow barcode assay using a portable, electronic imaging system suitable for digital archiving and transmission of assay results.

Conclusion

Using a photopatterning based method we detail a purely electronic format for a multiplexed lateral flow like assay. Requiring no grafting, pre-patterning or blocking steps, the UV-based immobilization of capture antigens relies on covalent bonding to a benzophenone group incorporated into a microchannel-filling LAVAgel. As such, a multiplexed barcode capture antigen pattern can be readily fabricated in a single, straight microchannel connecting two sample wells. Patterning of specific proteins is rapid and offers appreciable spatial resolution. Capture antigen photoimmobilization formed a lateral e-flow assay for specific detection of multiple human antibodies in sera, as is required for confirmatory diagnosis of HCV.[54] The total duration of the lateral e-flow assay was 60 min, whereas the HCV immunoblot strips require 240 to 600 min sample incubation yielding a total immunoblot strip assay time of 480 to 1200 min.[55]

To assess the potential for integration with a field-deployable fluorescence reader, we successfully integrated the lateral e-flow assay with a fluorescence detection enabled CellScope mobile reader. Digital imaging offers the potential for objective, standardized interpretation of a semi-quantitative readout, in contrast to the variability inherent in the current manual, subjective interpretation of multiplexed immunoblot strips.[55,56] Taken together, the lateral e-flow barcode assay and the fluorescence CellScope offer a versatile platform for implementing multiplexed immunoassays in point-of-care and near-patient settings.

Acknowledgements

The authors thank the Siebel Stem Cell Institute Postdoctoral Fellowship (to RL), the NSF Graduate Research Fellowship (to AS), NIH T32 training grant (T32AG000266 to the Buck Institute), and the NIH New Innovator Award (DP2OD007294 to AEH) for financial support. The authors thank members of the Herr Lab for helpful discussion, Jim C. Cheng, Ph.D. for generosity in assisting with the fabrication of the steel photomasks and Andy Lin for artistic expertise.

Notes and references

1 C. H. Self and D. B. Cook, *Curr. Opin. Biotechnol.*, 1996, **7**, 60–65.
2 R. M. Lequin, *Clin. Chem.*, 2005, **51**, 2415–2418.
3 G. Posthuma-Trumpie, J. Korf and A. Amerongen, *Anal. Bioanal. Chem.*, 2009, **393**, 569–582.
4 P. Yager, T. Edwards, E. Fu, K. Helton, K. Nelson, M. R. Tam and B. H. Weigl, *Nature*, 2006, **442**, 412–418.
5 G. S. Fiorini and D. T. Chiu, *BioTechniques*, 2005, **38**, 429–446.
6 C. D. Chin, V. Linder and S. K. Sia, *Lab Chip*, 2012, **12**, 2118–2134.
7 S. Vashist, O. Mudanyali, E. M. Schneider, R. Zengerle and A. Ozcan, *Anal. Bioanal. Chem.*, 2013, 1–15.
8 D. Tseng, O. Mudanyali, C. Oztoprak, S. O. Isikman, I. Sencan, O. Yaglidere and A. Ozcan, *Lab Chip*, 2010, **10**, 1787–1792.
9 H. Zhu, O. Yaglidere, T.-W. Su, D. Tseng and A. Ozcan, *Lab Chip*, 2011, **11**, 315–322.
10 D. N. Breslauer, R. N. Maamari, N. A. Switz, W. A. Lam and D. A. Fletcher, *PLoS One*, 2009, **4**, e6320.
11 A. H. C. Ng, U. Uddayasankar and A. R. Wheeler, *Anal. Bioanal. Chem.*, 2010, **397**, 991–1007.
12 A. Zubair, P. D. Burbelo, L. G. Vincent, M. J. Iadarola, P. D. Smith and N. Y. Morgan, *Biomed. Microdevices*, 2011, **13**, 1053–1062.
13 A. Salehi-Reyhani, J. Kaplinsky, E. Burgin, M. Novakova, A. J. Demello, R. H. Templer, P. Parker, M. A. A. Neil, O. Ces, P. French, K. R. Willison and D. Klug, *Lab Chip*, 2011, **11**, 1256–1261.
14 G. M. Whitesides, *Nature*, 2006, **442**, 368–373.
15 C. C. Lin, J. H. Wang, H. W. Wu and G. B. Lee, *JALA*, 2010, **15**, 253–274.
16 G. Hu, Y. Gao, P. Sherman and D. Li, *Microfluid. Nanofluid.*, 2005, **1**, 346–355.
17 A. T. Pereira, P. Novo, D. M. F. Prazeres, V. Chu and J. P. Conde, *Biomicrofluidics*, 2011, **5**, 014102.
18 A. W. Martinez, S. T. Phillips, E. Carrilho, S. W. Thomas, H. Sindi and G. M. Whitesides, *Anal. Chem.*, 2008, **80**, 3699–3707.
19 Y. Lu, W. Shi, J. Qin and B. Lin, *Electrophoresis*, 2009, **30**, 579–582.
20 P. B. Lillehoj, M.-C. Huang, N. Truong and C.-M. Ho, *Lab Chip*, 2013, **13**, 2950–2955.

21 S. Q. Wang, X. H. Zhao, I. Khimji, R. Akbas, W. L. Qiu, D. Edwards, D. W. Cramer, B. Ye and U. Demirci, *Lab Chip*, 2011, **11**, 3411–3418.
22 A. M. Tentori and A. E. Herr, *J. Micromech. Microeng.*, 2011, **21**, 054001.
23 M. A. Holden, S. Y. Jung and P. S. Cremer, *Anal. Chem.*, 2004, **76**, 1838–1843.
24 M. Y. Balakirev, S. Porte, M. Vernaz-Gris, M. Berger, J. P. Arie, B. Fouque and F. Chatelain, *Anal. Chem.*, 2005, 77, 5474–5479.
25 H. Nakajima, S. Ishino, H. Masuda, T. Nakagama, T. Shimosaka and K. Uchiyama, *Anal. Chim. Acta*, 2006, **562**, 103–109.
26 K. Shirai, B. Renberg, K. Sato, K. Mawatari, T. Konno, K. Ishihara and T. Kitamori, *Electrophoresis*, 2009, **30**, 4251–4255.
27 K. Jang, Y. Xu, K. Sato, Y. Tanaka, K. Mawatari and T. Kitamori, *Microchim. Acta*, 2012, **179**, 49–55.
28 R. A. O'Neill, A. Bhamidipati, X. H. Bi, D. Deb-Basu, L. Cahill, J. Ferrante, E. Gentalen, M. Glazer, J. Gossett, K. Hacker, C. Kirby, J. Knittle, R. Loder, C. Mastroieni, M. MacLaren, T. Mills, U. Nguyen, N. Parker, A. Rice, D. Roach, D. Suich, D. Voehringer, K. Voss, J. Yang, T. Yang and P. B. Vander Horn, *Proc. Natl. Acad. Sci. U. S. A.*, 2006, **103**, 16153–16158.
29 M. Petro, F. Svec and J. M. J. Frechet, *Biotechnol. Bioeng.*, 1996, **49**, 355–363.
30 D. S. Peterson, T. Rohr, F. Svec and J. M. J. Frechet, *Anal. Chem.*, 2003, **75**, 5328–5335.
31 F. Svec, *Electrophoresis*, 2006, **27**, 947–961.
32 T. C. Logan, D. S. Clark, T. B. Stachowiak, F. Svec and J. M. J. Frechet, *Anal. Chem.*, 2007, **79**, 6592–6598.
33 W. Lin and C. D. Skinner, *J. Sep. Sci.*, 2009, **32**, 2642–2652.
34 S. Fornera, P. Kuhn, D. Lombardi, A. D. Schluter, P. S. Dittrich and P. Walde, *ChemPlusChem*, 2012, 77, 98–101.
35 W. Zhan, G. H. Seong and R. M. Crooks, *Anal. Chem.*, 2002, **74**, 4647–4652.
36 S. Zimmermann, D. Fienbork, A. W. Flounders and D. Liepmann, *Sens. Actuators, B*, 2004, **99**, 163–173.
37 J. Heo and R. M. Crooks, *Anal. Chem.*, 2005, **77**, 6843–6851.
38 A. G. Lee, D. J. Beebe and S. P. Palecek, *Biomed. Microdevices*, 2012, **14**, 247–257.
39 M. K. Araz, A. A. Apori, C. M. Salisbury and A. E. Herr, *Lab Chip*, 2013, **13**, 3910–3920.
40 A. J. Hughes, R. K. C. Lin, D. M. Peehl and A. E. Herr, *Proc. Natl. Acad. Sci. U. S. A.*, 2012, **109**, 5972–5977.
41 A. Skandarajah, C. D. Reber, N. A. Switz and D. A. Fletcher, *PLoS One*, 2014, **9**, e96906.
42 A. Tapley, N. Switz, C. Reber, J. L. Davis, C. Miller, J. B. Matovu, W. Worodria, L. Huang, D. A. Fletcher and A. Cattamanchi, *J. Clin. Microbiol.*, 2013, **51**, 1774–1778.
43 D. J. Throckmorton, T. J. Shepodd and A. K. Singh, *Anal. Chem.*, 2002, **74**, 784–789.
44 A. E. Herr and A. K. Singh, *Anal. Chem.*, 2004, **76**, 4727–4733.
45 A. A. Apori and A. E. Herr, *Anal. Chem.*, 2011, **83**, 2691–2698.
46 G. Dorman and G. D. Prestwich, *Biochemistry*, 1994, **33**, 5661–5673.
47 A. J. Hughes and A. E. Herr, *Proc. Natl. Acad. Sci. U. S. A.*, 2012, **109**, 21450–21455.
48 D. Dussault and P. Hoess, Noise performance comparison of ICCD with CCD and EMCCD cameras, *Proc. SPIE*, 2004, **5563**, 195–204.
49 T. M. Squires, R. J. Messinger and S. R. Manalis, *Nat. Biotechnol.*, 2008, **26**, 417–426.
50 M. A. Kapil and A. E. Herr, *Anal. Chem.*, 2014, **86**, 2601–2609.
51 J. Versalovic, *Manual of Clinical Microbiology*, ASM Press, Washington DC, 2011.
52 P. Martin, F. Fabrizi, V. Dixit, S. Quan, M. Brezina, E. Kaufman, K. Sra, R. DiNello, A. Polito and G. Gitnick, *J. Clin. Microbiol.*, 1998, **36**, 387–390.
53 F. Fabrizi, P. Martin, V. Dixit, S. Quan, M. Brezina, E. Kaufman, K. Sra, M. Mousa, R. DiNello, A. Polito and G. Gitnick, *Am. J. Nephrol.*, 2001, **21**, 104–111.
54 A. S. Lok and N. T. Gunaratnam, *Hepatology*, 1997, **26**, 48S–56S.
55 www.fda.gov. Chiron RIBA HCV 3.0 Strip Immunoblot Assay and P. I. Product Information.
56 R. www.who.int Hepatitis C Assays: Operational Characteristics (PHASE I), July 2001.

Electronic Supplementary Material (ESI) for Lab on a Chip.

Supplemental Information

The photopatterned barcode capture antigen locations were validated by probing with primary and secondary antibodies.

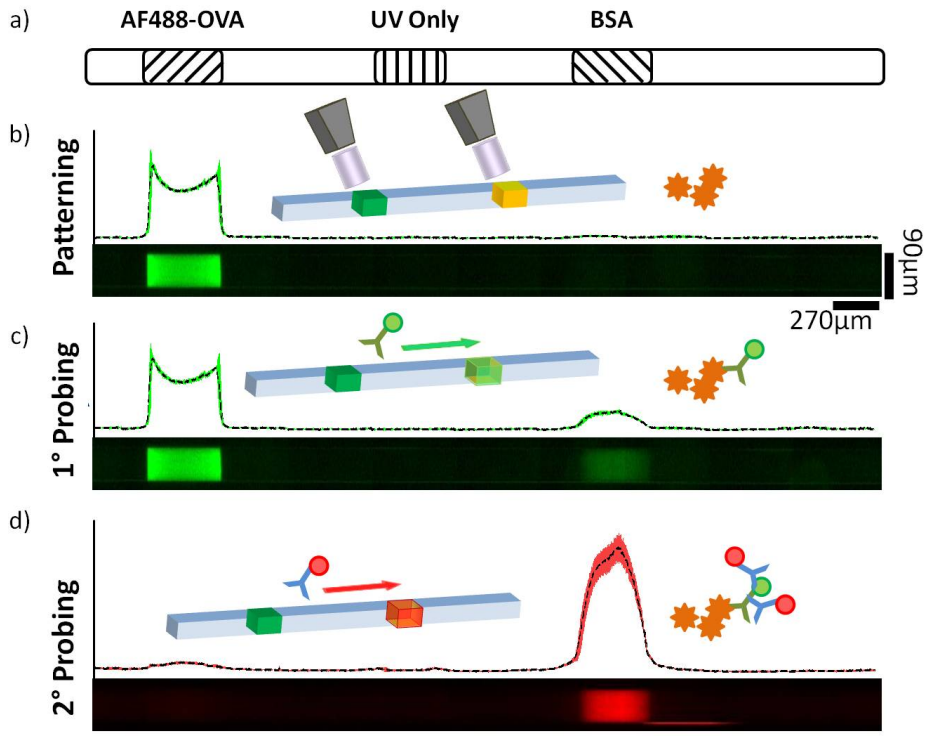

Figure S1. **Validation of protein barcode patterning**. a) Schematic of capture antigen barcode layout. As a negative control, a barcode region exposed to UV illumination with no proteins present is employed. b) Micrograph and line scan of the barcode channel after protein patterning. c) Micrograph and line scan after loading of fluorescently labeled primary antibody. d) Micrograph and line scan after loading of fluorescently labeled secondary antibody.

Increased UV dose decreases fluorescence signal from AlexaFluor-labeled proteins

To scrutinize the impact of UV illumination on the fluorescence signal from AlexaFluor-labeled proteins, individual wells of standard microwell plate were filled with 60uL of BSA-AF488 solution. The microwell plate was a black, flat bottomed, polystyrene 96well plates from Corning. The solution was then illuminated using the Hamamatsu UV source for 0s, 1s, 5s, 10s, 20s, 40s and 60s using the 20% power setting. Each time point was tested in triplicate. The UV exposure durations were selected based on the durations employed in the barcode assay. Fluorescence signal from each microwell containing a 1uM solution of BSA-AF488 was measured using a Tecan Infinite M200 Pro microplate reader before and after UV exposure, as shown in Figure S2.

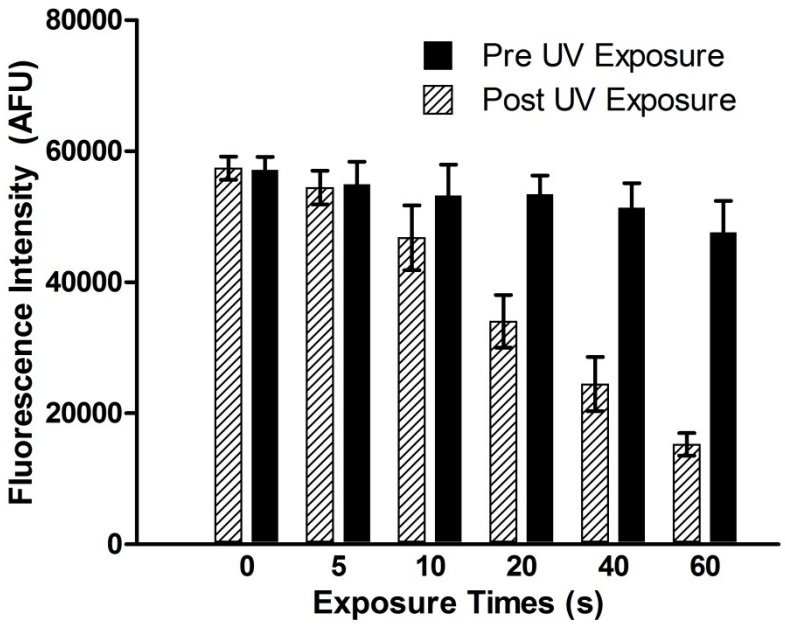

Figure S2. **UV photobleaching of fluorescently labeled proteins**. Microplate reader collected fluorescence signal from AF488-labelled BSA before and after UV illumination shows notable fluorescence signal decrease with increasing UV dose.

While the effective UV dose applied to microwell plate is different than that applied to the microdevice during UV photopatterning, the data support the working conclusion that UV dose can impact fluorescence of the AlexaFluor dyes used here. During photopatterning of the barcode assay, the light guide is placed in proximity to the microchannel (<1mm displacement). For the microwell plate experiment, physical limitations locate the light guide ~9mm from the well floor. Thus, the UV dose applied to the microwells is less than the dose applied to the barcode microchannels. To increase the UV dose in the microwell system, we increased the UV illumination duration to 40s and 60s, yielding increased UV dose and concomitant decrease in AlexaFluor488 signal, as observed in the barcode assay.